KSME

Springer

Journal of Mechanical Science and Technology 35 (7) 2021

Original Article
DOI 10.1007/s12206-021-0621-1

Keywords:
· Potential solution
· Sloshing
· Rectangular tank
· Tank velocity profile

Correspondence to:
Dongjoo Kim
kdj@kumoh.ac.kr

Citation:
Kim, D. (2021). Potential solution for sloshing in a horizontally moving rectangular tank and design of tank velocity profile. Journal of Mechanical Science and Technology 35 (7) (2021) 2981~2988. http://doi.org/10.1007/s12206-021-0621-1

Received February 19th, 2021
Revised March 25th, 2021
Accepted March 30th, 2021

† Recommended by Editor
Yang Na

Potential solution for sloshing in a horizontally moving rectangular tank and design of tank velocity profile

Dongjoo Kim

Department of Mechanical Engineering, Kumoh National Institute of Technology, Gumi, Gyeongbuk 39177, Korea

Abstract Sloshing makes it challenging to transport liquid-containing systems fast. Accurate prediction and effective suppression of sloshing are essential in many industrial applications. Two different methods are commonly used to numerically investigate the sloshing phenomenon: CFD simulation and equivalent mechanical model. Due to each method's pros and cons, the solutions based on potential flow theory can be a good alternative for sloshing study. However, previous studies mostly focused on sloshing under sinusoidal oscillations, and only a little effort has been made to understand and suppress the sloshing under point-to-point movements. In this study, potential solutions for sloshing in a rectangular tank under horizontal point-to-point movements are newly derived and verified by comparing with the present CFD results. So far, the velocity profile of liquid-containing tanks has attracted little attention from the sloshing suppression point of view. However, simply a suitable choice of velocity profile (acceleration/deceleration duration) can lead to much-reduced sloshing. Results show that the present potential solutions are beneficial for designing the tank velocity profile for minimum residual sloshing under a given condition. It is also shown that the acceleration/deceleration duration affects the sloshing amplitude more significantly than its magnitude.

1. Introduction

In many industrial applications, high-speed position control of a liquid-containing tank causes undesirable liquid vibrations called 'sloshing' [1, 2]. The sloshing poses a control challenge in fast maneuvering and accurate positioning of liquid tanks. One of the problems caused by violent sloshing is that the liquid comes out of open tanks. Therefore, it is important to accurately predict [3, 4] and effectively suppress [5-7] the sloshing in moving tanks.

To predict the sloshing phenomenon numerically, CFD (computational fluid dynamics) simulation and analysis based on equivalent mechanical models are commonly used. In the former, the governing equations for fluid motions are directly solved to provide an accurate solution, but it requires relatively much CPU time. On the other hand, in the latter, fluid motions are approximated based on an equivalent mechanical model such as a mass-spring or pendulum system [1, 7]. Therefore, the solution, though quickly obtained, is not as accurate as CFD results. As an alternative method, potential solutions can be considered if available because they are more accurate than the mechanical model and more efficient than CFD simulations.

Previous studies mainly focused on the sloshing under sinusoidal oscillation of liquid tanks (Fig. 1(a)), caused by unwanted external forces such as earthquakes and sea waves [4, 5, 8, 9]. On the other hand, relatively little attention has been paid to the sloshing under point-to-point movements (Fig. 1(b)) for positioning the tank. Even after the tank stops through this movement, the free surface continues to oscillate, as shown later in Sec. 4. This residual vibration needs to be suppressed to immediately move on to the following process, but little knowledge has been obtained for this type of sloshing. As a result, potential solutions for sloshing under non-sinusoidal motions of tanks (e.g., triangular and trapezoidal profiles of tank velocity) have

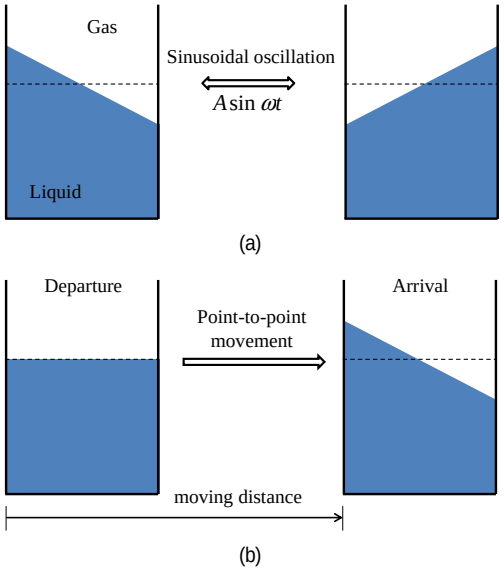

Fig. 1. Two different types of sloshing problems: (a) sinusoidal oscillation; (b) point-to-point movement.

not been developed, to the best of the author's knowledge.

The purpose of this study is to derive potential solutions for sloshing in rectangular tanks moving horizontally from a point to another, and then verify them from a comparison with the present CFD results. The potential solutions are given for triangular and rectangular velocity profiles as a representative example, but the general solution proposed here can be formulated into a specific form for any other profile. We also aim to show that present potential solutions are beneficial for designing the tank velocity profile for minimum residual sloshing, and merely the right choice of acceleration/deceleration duration can result in much-reduced sloshing.

2. Potential solution

2.1 General solution

We consider a two-dimensional, rectangular, open tank in which a fluid is filled up to the height h from the tank bottom, as shown in Fig. 2. The tank of length L is forced to undergo a horizontal movement toward another position. A Cartesian coordinate system is defined so that its origin is located at the center of the undisturbed free surface. Here, x and y denote the horizontal and vertical directions, respectively.

We assume that the flow is inviscid, incompressible, irrotational, and the displacement of the free surface is small. Under these assumptions, there exists a velocity potential Φ that satisfies the Laplace equation,

$$\nabla^2\Phi = 0, \tag{1}$$

in the fluid domain [8]. Neglecting surface tension, we can specify the linearized dynamic and kinematic free-surface conditions as

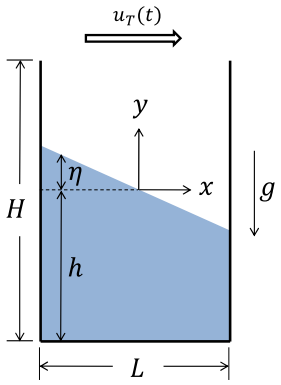

Fig. 2. Coordinate system for sloshing in a horizontally moving tank.

$$\frac{\partial\Phi}{\partial t} + g\eta = 0 \quad \text{on} \quad y = \eta(x,t), \tag{2}$$

$$\frac{\partial\eta}{\partial t} = \frac{\partial\Phi}{\partial y} \qquad \text{on} \quad y = \eta(x,t). \tag{3}$$

Here g is the acceleration of gravity and η is the free surface elevation measured from the undisturbed free surface. On the side and bottom walls of the tank, the potential satisfies the following conditions:

$$\frac{\partial\Phi}{\partial x} = u_T(t) \quad \text{on} \quad x = \pm L/2, \tag{4}$$

$$\frac{\partial\Phi}{\partial y} = 0 \qquad \text{on} \quad y = -h. \tag{5}$$

The total potential Φ can be decomposed into two parts ($\Phi = \phi_{tank} + \phi$). The potentials ϕ_{tank} and ϕ denote the tank motion and the fluid motion relative to the tank, respectively. In this study, $\phi_{tank} = u_T x$ because the tank is subject to horizontal movement. The governing equation and boundary conditions (Eqs. (1)-(5)) can be rewritten for the potential ϕ as follows:

$$\nabla^2\phi = 0, \tag{6}$$

$$\frac{\partial\phi}{\partial t} + g\eta = -\frac{du_T}{dt}x \quad \text{on} \quad y = \eta(x,t), \tag{7}$$

$$\frac{\partial\eta}{\partial t} = \frac{\partial\phi}{\partial y} \quad \text{on} \quad y = \eta(x,t), \tag{8}$$

$$\frac{\partial\phi}{\partial x} = 0 \quad \text{on} \quad x = \pm\frac{L}{2}, \tag{9}$$

$$\frac{\partial\phi}{\partial y} = 0 \quad \text{on} \quad y = -h. \tag{10}$$

The velocity potential ϕ can be analytically derived by the separation of variables. Inserting $\phi(x,y,t) = X(x)Y(y)\dot{B}(t)$ into Eq. (6) produces

$$\frac{d^2X}{dx^2} + k^2X = 0, \quad \frac{d^2Y}{dx^2} - k^2Y = 0, \tag{11}$$

with the separation constant k. Applying the boundary conditions of Eqs. (9) and (10) gives us

$$\phi = \sum_{n=1}^{\infty} \sin k_n x \cosh k_n (y+h) \dot{B}_n(t) \tag{12}$$

where $k_n = (2n-1)\pi / L$.

It can be shown that the following Fourier series expansion is valid.

$$x = \sum_{n=1}^{\infty} \frac{4}{L} \frac{(-1)^{n-1}}{k_n^2} \sin k_n x. \tag{13}$$

Putting Eqs. (12) and (13) into Eq. (7) leads to

$$\ddot{B}_n + \omega_n^2 B_n = \frac{1}{\cosh k_n h} \frac{4}{L} \frac{(-1)^{n-1}}{k_n^2} \left(-\frac{du_T}{dt} \right) \tag{14}$$

where the angular frequency of natural sloshing ω_n is defined as

$$\omega_n^2 = g k_n \tanh k_n h. \tag{15}$$

With the initial conditions ($B_n(0) = \dot{B}_n(0) = 0$), we can obtain $B_n(t)$ from Eq. (14). Applying the Laplace transform to Eq. (14) gives us the general solution for $B_n(s)$.

$$B_n(s) = \frac{1}{\cosh k_n h} \frac{4}{L} \frac{(-1)^n}{k_n^2} \frac{1}{s^2 + \omega_n^2} a_T(s), \tag{16}$$

where a_T denotes the acceleration of the tank. The velocity potential ϕ is now known from Eq. (12) and then the perturbed elevation $\eta(x,s)$ can be obtained from Eq. (8).

$$\eta(x,s) = \sum_{n=1}^{\infty} \sin k_n x \frac{4}{gL} \frac{(-1)^n}{k_n^2} \frac{\omega_n^2}{s^2 + \omega_n^2} a_T(s). \tag{17}$$

Putting $x = -L/2$ into Eq. (17) leads to the elevation at the left wall in the Laplace domain.

$$\eta_{left}(s) = \sum_{n=1}^{\infty} \frac{C_n \omega_n^2}{s^2 + \omega_n^2} a_T(s) = \sum_{n=1}^{\infty} \frac{4L}{g(2n-1)^2 \pi^2} \frac{\omega_n^2}{s^2 + \omega_n^2} a_T(s). \tag{18}$$

Here the coefficient $C_n = 4L / g(2n-1)^2 \pi^2$ shows the contribution of the specific (n-th) mode to the perturbed free-surface elevation. The modal contribution coefficient C_n is inversely proportional to $(2n-1)^2$ and thus it is small in higher modes as compared to lower modes. The limited accuracy of equivalent mechanical models is generally caused by the lack of information about the modal contribution corresponding to C_n.

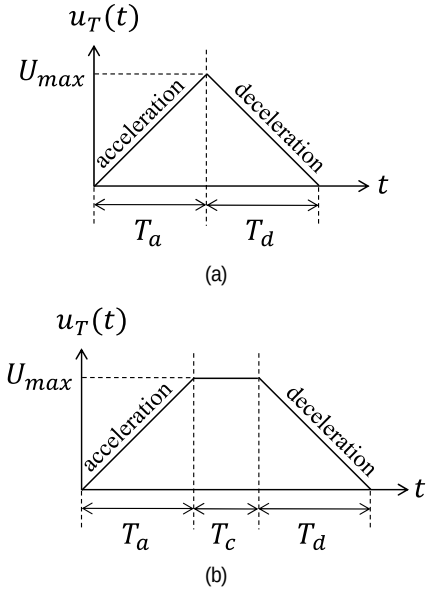

Fig. 3. Representative profiles of tank velocity: (a) triangle; (b) trapezoid.

Note that only the odd modes appear in Eq. (18).

The final solution in the time domain is calculated by taking the inverse Laplace transform of Eq. (18).

$$\eta_{left}(t) = L^{-1}\{\eta_{left}(s)\} = L^{-1}\left\{ \sum_{n=1}^{\infty} \frac{4L}{g(2n-1)^2 \pi^2} \frac{\omega_n^2}{s^2 + \omega_n^2} a_T(s) \right\}. \tag{19}$$

This solution in a general form can be formulated more specifically when the tank velocity profile is given, as shown in Sec. 2.2. The left free-surface elevation will be used to measure sloshing strength in Sec. 4.

2.2 Solution for triangular and trapezoidal velocity profiles

Fig. 3 shows two representative profiles of tank velocity for transportation: triangular and trapezoidal ones. We first consider the triangular profile shown in Fig. 3(a). The stationary tank starts to move at $t = 0$ and accelerates for a period of time T_a until it reaches the maximum velocity U_{max}. Then the tank decelerates for a duration of T_d so that it finally stops.

Using unit ramp function $r(t)$ and unit step function $u(t)$, we can write the tank velocity and the tank acceleration as

$$\begin{aligned} u_T(t) = {} & \frac{U_{max}}{T_a} \{ r(t) - r(t - T_a) \} \\ & + \frac{U_{max}}{T_d} \{ -r(t - T_a) + r(t - T_a - T_d) \}, \end{aligned} \tag{20}$$

$$\begin{aligned} a_T(t) = {} & \frac{U_{max}}{T_a} \{ u(t) - u(t - T_a) \} \\ & + \frac{U_{max}}{T_d} \{ -u(t - T_a) + u(t - T_a - T_d) \}, \end{aligned} \tag{21}$$

$$a_T(s)=\frac{U_{max}}{T_a}\left\{\frac{1}{s}-\frac{e^{-T_a s}}{s}\right\}+\frac{U_{max}}{T_d}\left\{-\frac{e^{-T_a s}}{s}+\frac{e^{-(T_a+T_d)s}}{s}\right\}. \quad (22)$$

Putting Eq. (22) into Eq. (19) and taking the inverse Laplace transform leads to

$$\begin{aligned}\eta_{left}(t)=&\frac{U_{\max}}{T_a}\sum_{n=1}^{\infty}\frac{4L}{g(2n-1)^2\pi^2}\left\{(1-\cos\omega_n t)\right.\\&\left.-(1-\cos\omega_n(t-T_a))u(t-T_a)\right\}\\&+\frac{U_{\max}}{T_d}\sum_{n=1}^{\infty}\frac{4L}{g(2n-1)^2\pi^2}\left\{-(1-\cos\omega_n(t-T_a))u(t-T_a)\right.\\&\left.+(1-\cos\omega_n(t-T_a-T_d))u(t-T_a-T_d)\right\}. \quad (23)\end{aligned}$$

The perturbed free-surface elevation is a sum of responses for an infinite number of sloshing modes. From Eq. (23), it is clear that the sloshing amplitude is affected by the acceleration and deceleration duration (T_a & T_d) as well as their magnitude ($U_{\max}/T_a$ & $U_{\max}/T_d$). When $T_a=m_1T_n(m_1=1,2,3\ldots)$ and $t>T_a$, the first two terms of the *n*-th mode in the right-hand side are canceled out. Similarly, when $T_d=m_2T_n$ ($m_2=1,2,3\ldots$) and $t>T_a+T_d$, the remaining two terms of the *n*-th mode can also be canceled out. Note that irrespective of U_{max}/T_a and U_{max}/T_d, the residual free-surface oscillation of the *n*-th mode can be eliminated by a careful choice of acceleration and deceleration duration. On the other hand, when $T_a=(m_1+1/2)T_n$ and $T_d=(m_2+1/2)T_n$, the residual free-surface oscillation of the *n*-th mode can be much enhanced. Because the 1st mode makes the most considerable contribution to sloshing as explained in Sec. 2.1, it has to be considered in determining the acceleration and deceleration duration rather than any other modes. This important understanding obtained from the potential solution will be verified by comparing with the present CFD results performed for the same conditions.

In a similar way, we can obtain the potential solution for a trapezoidal profile shown in Fig. 3(b). The tank experiences a sequence of acceleration, constant velocity, and deceleration, respectively, for the time span of T_a, T_c and T_d. The potential solution is easily derived as

$$\begin{aligned}\eta_{left}(t)=&\frac{U_{\max}}{T_a}\sum_{n=1}^{\infty}\frac{4L}{g(2n-1)^2\pi^2}\left\{(1-\cos\omega_n t)\right.\\&\left.-(1-\cos\omega_n(t-T_a))u(t-T_a)\right\}\\&+\frac{U_{\max}}{T_d}\sum_{n=1}^{\infty}\frac{4L}{g(2n-1)^2\pi^2}\left\{-(1-\cos\omega_n(t-T_a-T_c))u(t-T_a-T_c)\right.\\&\left.+(1-\cos\omega_n(t-T_a-T_c-T_d))u(t-T_a-T_c-T_d)\right\}. \quad (24)\end{aligned}$$

3. Numerical methods

3.1 Test problem

CFD simulations are performed for the following conditions to verify the present potential solutions. A rectangular tank of length $L=0.2$ m is partially filled with water, and its top is open to the ambient air as shown in Fig. 2. The height of the tank H is 0.3 m and the initial water height h is 0.2 m. The tank moves horizontally from a point to another with a triangular velocity profile shown in Fig. 3(a). In this study, the deceleration duration is set to be the same as that of acceleration ($T_d=T_a$) for all the test cases. Therefore, the deceleration magnitude is also the same as that of acceleration.

Table 1. Characteristics of the first three odd natural modes.

n	ω_n (rad/s)	T_n (s)	C_n ($\times10^{-3}$ s^2)
1	12.390	0.507	8.263
2	21.501	0.292	0.918
3	27.757	0.226	0.331

As explained in Sec. 2.2, there are two different parameters to affect the sloshing amplitude significantly: acceleration duration and acceleration magnitude. To understand the effect of the parameters on sloshing, two different situations were investigated. In the first case, the acceleration magnitude is fixed to be 1 m/s^2 and a parametric study on the acceleration duration T_a is performed to find an optimal condition for minimum sloshing. In the second case, the tank's traveling distance is fixed to be 0.25 m and another parametric study is repeated for the acceleration duration. In this practical situation, both the acceleration duration and the acceleration magnitude change simultaneously.

In designing a tank velocity profile, it is crucial to know the natural sloshing frequency (or period), especially the first and subsequent low-mode frequencies making a significant contribution to sloshing. Table 1 summarizes the natural frequencies, periods, and modal contribution coefficients C_n of several lower modes. For example, the natural periods of the first three odd modes are 0.507 s, 0.292 s, and 0.226 s, respectively.

3.2 CFD details

The water and air flows inside the tank are simulated with the assumption of two-dimensional, inviscid, and incompressible flow for comparison with the present potential solution. The unsteady velocity and pressure fields are obtained by using a commercial CFD solver, Fluent. To predict the two-phase flow and capture the motion of the free surface between water and air, we use a VOF (volume of fluid) two-phase flow model. Like many previous studies [4, 9, 10], the coordinate system is chosen to move with the tank velocity. Therefore, the governing equations can be written as

$$\frac{\partial\rho}{\partial t}+\frac{\partial}{\partial x_i}(\rho u_i)=0, \quad (25)$$

$$\frac{\partial}{\partial t}(\rho u_i)+\frac{\partial}{\partial x_j}(\rho u_i u_j)=-\frac{\partial p}{\partial x_i}+\rho f_i, \quad (26)$$

$$\frac{\partial\alpha}{\partial t}+\frac{\partial}{\partial x_i}(\alpha u_i)=0. \quad (27)$$

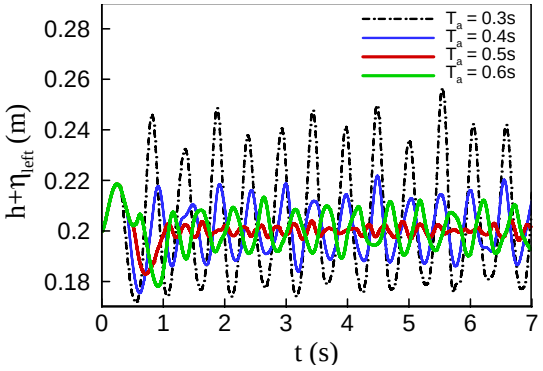

Fig. 4. Time history of water level at the left wall (CFD results).

Here, x_i, u_i, p, and ρ denote the Cartesian coordinates, velocity components, pressure, and fluid density, respectively. Note that ρ is the volume-averaged value according to the VOF method [11]. The external force per unit mass f_i consists of gravitational force and translational inertia force: $f_1 = -du_T / dt$ and $f_2 = -g$. The scalar function α in Eq. (27) is defined as the ratio of liquid volume to cell volume and it ranges from 0 to 1. $\alpha = 0$ indicates that the cell is full of air, whereas $\alpha = 1$ denotes that the cell is full of water.

The computational domain size is 0.2 m $(x) \times$ 0.3 m (y) corresponding to the inside of the tank. The no-penetration boundary condition is used on the tank walls, and the pressure is prescribed to be zero (i.e., atmospheric pressure) at the top boundary. The number of grid points and the time step size are determined from a resolution test. The numbers of cells used are 100 and 150, respectively, in x and y directions, and the time step size is $\Delta t = 0.001$ s.

4. Results

4.1 Constant acceleration/deceleration

The cases of constant acceleration/deceleration magnitude ($|a_T| = 1$ m/s^2) with $T_a = T_d$ are first considered in this section. The acceleration duration T_a varies from 0 to 2 s, which covers approximately four times the first mode period of natural sloshing. The tank's moving distance S_T also changes with the acceleration duration ($S_T = a_T T_a^2$).

Fig. 4 shows the time history of water level at the left wall obtained from CFD simulation for various acceleration duration. One may expect similar strength of free-surface fluctuations because the acceleration magnitude is the same for all the cases. However, there exists a large difference in the fluctuations depending on the acceleration duration. Among the four cases considered, the case of $T_a = 0.3$ s shows the largest fluctuations. As T_a increases from $T_a = 0.3$ s, the fluctuations decrease until they become very small for $T_a = 0.5$ s. With a further increase, however, the fluctuations start to increase. These observations are also seen in Fig. 5, illustrating temporal variations of water-air interface using the VOF scalar function α. Remember that the 1st mode period of natural sloshing is $T_1 = 0.507$ s. In the least sloshing case ($T_a = 0.5$ s), T_a is very close to T_1. On the other hand, in the most severe sloshing case ($T_a = 0.3$ s), T_a is the closest to $T_1 / 2$. This dependency on the acceleration duration is consistent with the present solution of Eq. (23) and discussions in Sec. 2.2.

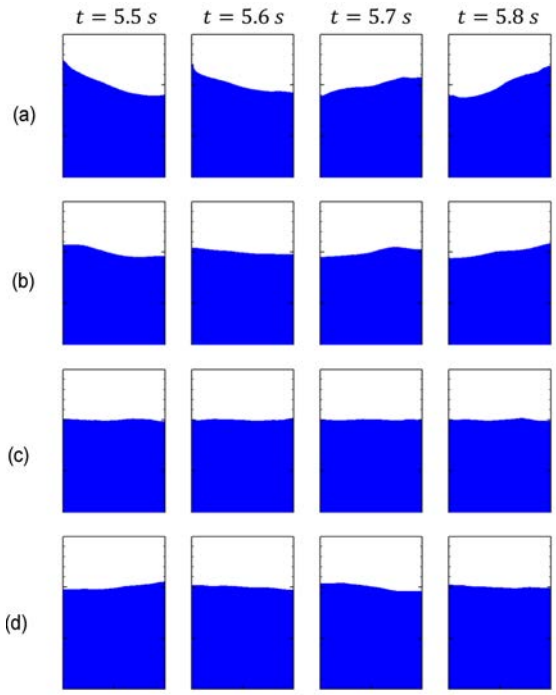

Fig. 5. Temporal variation of water-air interface for various acceleration duration: (a) $T_a = 0.3$ s; (b) $T_a = 0.4$ s; (c) $T_a = 0.5$ s; (d) $T_a = 0.6$ s.

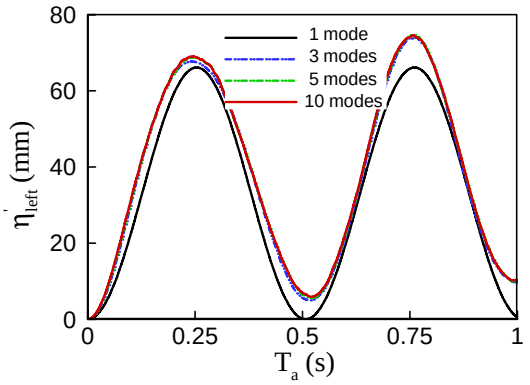

Fig. 6. Dependency of sloshing amplitude on the number of modes considered in the potential solution.

Because the potential solution of Eq. (23) includes an infinite number of modes, the convergence according to the number of modes for summation is tested. Higher modes contribute relatively little compared to lower modes, and thus some of the low modes are predominant. Fig. 6 shows the dependency of sloshing amplitude on the number of odd modes considered in Eq. (23). The sloshing amplitude is measured by the difference between the maximum and minimum water elevation at the left wall ($\eta_{left}^{max} - \eta_{left}^{min}$) after the tank stops. As can be seen, there is

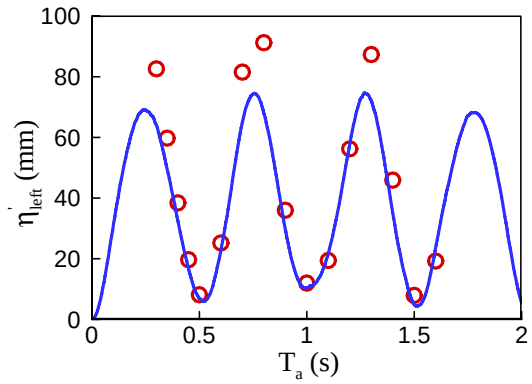

Fig. 7. Comparison of potential and CFD solutions for residual sloshing amplitude at the left wall (constant acceleration case): ○, CFD; —, potential solution.

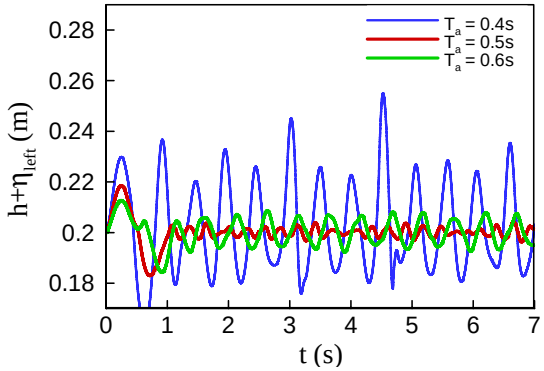

Fig. 8. Time history of water level at the left wall (CFD results).

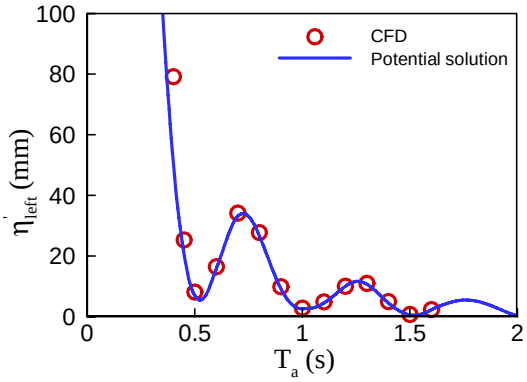

Fig. 9. Comparison of potential and CFD solutions for residual sloshing amplitude at the left wall (constant moving-distance case).

little difference between 5-modes and 10-modes cases, meaning that the sloshing amplitude is determined mainly by the first five odd modes. In the following analysis of the potential solution, however, 100 modes are used due to fast calculation.

Fig. 7 shows the sloshing amplitude of the potential solution as a function of the acceleration duration. CFD results are also included for comparison. The potential solution overall agrees well with the CFD results, particularly near $T_a \approx T_1$, $T_a \approx 2T_1$, and $T_a \approx 3T_1$. The discrepancy between the two solutions increases as the sloshing becomes violent. This is because the potential solution is based on linear assumptions, and its accuracy decreases as the nonlinearity gets stronger. Unless the sloshing is violent, the amplitude of residual sloshing can be easily predicted using the potential solution derived in this study.

4.2 Constant moving distance

Now, we consider a more practical problem where the target distance of tank movement (S_T) and the maximum traveling time ($T_{\max}$) allowed are given. Suppose we want to find the optimum acceleration duration $T_a (= T_d \le T_{\max}/2)$ of the triangular velocity profile for minimum residual sloshing. In this scenario, the acceleration magnitude $a_T (= S_T / T_a^2)$ changes with the acceleration duration T_a, so the two parameters T_a and a_T depend on each other. Under the assumption of $S_T = 0.25$ m, $T_{max} = 1.2$ s, four different cases ($T_a = 0.3$~0.6 s) are simulated. However, the result of $T_a = 0.3$ s is not included here because some of the water is spilt out of the tank during the simulation.

Fig. 8 shows the water level history at the left wall obtained from the present CFD results. Interestingly, the minimum residual sloshing is not found at the slowest movement ($T_a = 0.6$ s), but at $T_a = 0.5$ s. The acceleration magnitudes are 1 m/s^2 and 0.694 m/s^2, respectively, for $T_a = 0.5$ s and $T_a = 0.6$ s. This result can be explained by the fact that the exact match of T_a and T_1 can completely eliminate the most energetic mode (1st mode) of sloshing, regardless of acceleration magnitude. In the case of $T_a = 0.5$ s, T_a almost matches T_1 resulting in more reduced sloshing than for $T_a = 0.6$ s.

Fig. 9 shows the sloshing amplitude of the potential solution as a function of the acceleration duration, together with the CFD results for comparison. Again, the potential solution agrees well with the CFD results, allowing us to decide the acceleration duration for minimum sloshing based on the potential solution. The sloshing amplitude shows local minima at $T_a = T_1$, $2T_1$, and $3T_1$, while it shows local maxima at $T_a = 1.5T_1$, $2.5T_1$, and $3.5T_1$. Under the condition of constant moving distance, the value of local maxima decreases with T_a unlike in Fig. 7 because the acceleration magnitude also decreases. When the maximum traveling time allowed for tank transportation $T_{\max}$ is given, $T_{\max}/2$ is not generally the best choice as the acceleration duration for minimum residual sloshing. Among the multiples of the 1st mode natural period smaller than $T_{\max}/2$, the largest one (nearest to $T_{\max}/2$) is the optimum value for minimum residual sloshing.

4.3 Effect of viscosity

The present potential solution was confirmed in the previous sections by comparing it with the CFD solutions for inviscid flow. One may question if the potential solution is useful for designing the tank velocity profile, even for realistic situations of viscous flow. So, additional CFD simulations with the viscosity

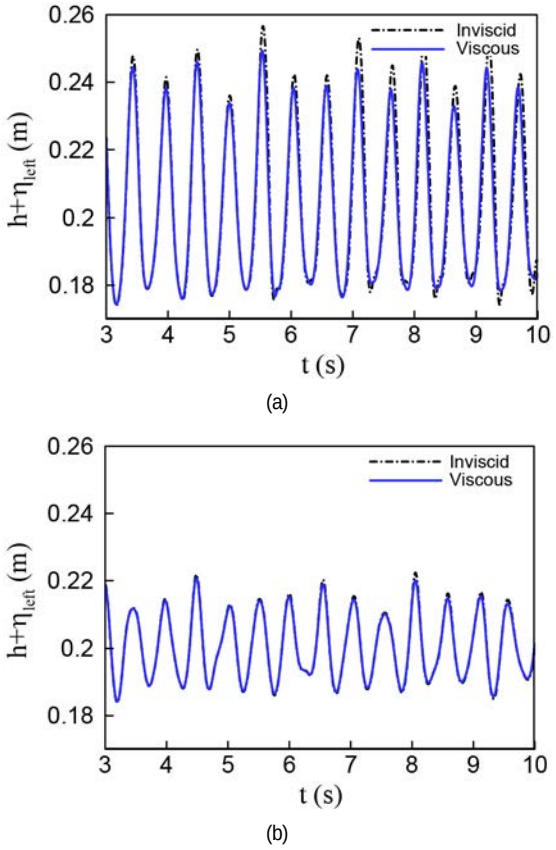

Fig. 10. Comparison of inviscid and viscous CFD results for water level at the left wall: (a) $T_a = 0.3$ s; (b) $T_a = 0.4$ s.

effect included are performed for the cases considered in Sec. 4.1. In the viscous flow simulations, the no-slip boundary condition is prescribed at the walls.

Comparisons between the inviscid and viscous flow results are made in Fig. 10 for the water level history at the left wall. In the case of severe sloshing at $T_a = 0.3$ s, the fluid viscosity makes the free-surface fluctuations reduced to some extent. On the other hand, when the sloshing is less severe at $T_a = 0.4$ s, the viscosity effect is negligible. Therefore, the present potential solution is still valid for predicting mild water sloshing in the air, and so it can be used to design the tank velocity profile for minimum residual sloshing.

5. Conclusions

Non-sinusoidal horizontal transportation of liquid tanks is prevalent in various industrial applications, so the sloshing under this condition was investigated based on the potential theory and CFD simulations. The potential solution for free-surface elevation was newly derived in a general form for a rectangular tank moving horizontally from one point to another. More specific equations were also developed for two representative profiles of tank velocity: triangle and trapezoid. The present solutions were verified by comparing them with the present CFD results under the inviscid flow assumption.

So far, the liquid tank's velocity profile has received little attention from the sloshing suppression point of view. However, we showed that the acceleration/deceleration duration of the velocity profile affects the sloshing amplitude more than its magnitude. The acceleration duration has to be a multiple of the first mode period of natural sloshing to minimize the residual sloshing. Importantly, merely a right choice of acceleration/deceleration duration can lead to much-reduced sloshing. The present potential solutions will help design the tank velocity profile for minimum sloshing and elucidate the underlying reasons for reduced or enhanced sloshing for different tank velocity profiles.

Acknowledgments

This research was supported by Kumoh National Institute of Technology.

Nomenclature

a_T	: Tank acceleration
C_n	: Modal contribution coefficient
h	: Initial water height
L	: Tank length
T_a	: Acceleration duration
T_d	: Deceleration duration
T_{max}	: Maximum travelling time allowed
T_n	: n -th mode period of natural sloshing
U_{max}	: Maximum velocity
u_T	: Tank velocity
α	: Scalar function for VOF model
Φ	: Total potential for fluid flow
ϕ_{tank}	: Potential for tank motion
ϕ	: Potential for fluid motion relative to tank
η_{left}	: Perturbed elevation at the left wall
η'_{left}	: Difference between maximum and minimum water elevations at the left wall
ω_n	: Angular frequency of natural sloshing

References

[1] R. A. Ibrahim, *Liquid Sloshing Dynamics: Theory and Applications*, Cambridge University Press, Cambridge, United Kingdom (2005).

[2] O. M. Faltinsen and A. N. Timokha, *Sloshing*, Cambridge University Press, New York, USA (2009).

[3] S. Rebouillat and D. Liksonov, Fluid-structure interaction in partially filled liquid containers: a comparative review of numerical approaches, *Computers and Fluids*, 39 (5) (2010) 739-746.

[4] D. Liu and P. Lin, A numerical study of three-dimensional liquid sloshing in tanks, *J. of Computational Physics,* 227 (8) (2008) 3921-3939.

[5] D. Liu and P. Lin, Three-dimensional liquid sloshing in a tank with baffles, *Ocean Engineering,* 36 (2) (2009) 202-212.

[6] A. Aboel-Hassan, M. Arafa and A. Nassef, Design and optimization of input shapers for liquid slosh suppression, *J. of Sound and Vibration*, 320 (1-2) (2009) 1-15.
[7] K. Yano and K. Terashima, Robust liquid container transfer control for complete sloshing suppression, *IEEE Transactions on Control Systems Technology*, 9 (3) (2001) 483-493.
[8] G. X. Wu, Q. W. Ma and R. E. Taylor, Numerical simulation of sloshing waves in a 3D tank based on a finite element method, *Applied Ocean Research*, 20 (6) (1998) 337-355.
[9] B.-F. Chen and R. Nokes, Time-independent finite difference analysis of fully non-linear and viscous fluid sloshing in a rectangular tank, *J. of Computational Physics*, 209 (1) (2005) 47-81.
[10] H. Akyildiz and N. E. Unal, Sloshing in a three-dimensional rectangular tank: numerical simulation and experimental validation, *Ocean Engineering*, 33 (6) (2006) 2135-2149.
[11] C. W. Hirt and B. D. Nichols, Volume of fluid (VOF) method for the dynamics of free boundaries, *J. of Computational Physics*, 39 (1) (1981) 201-225.

Dongjoo Kim is a Professor of Mechanical Engineering at Kumoh National Institute of Technology. He received his Ph.D. in Mechanical Engineering from Seoul National University. His research interests include computational fluid dynamics, flow control, multiphase flow, and particle dynamics.